Lunar occultation observations and a study of

cosmic size evolution of extragalactic radio sources

Ashok Kumar Singal

Radio Astronomy Centre

Tata Institute of Fundamental Research

A thesis submitted for the Ph.D. degree

of the University of Bombay

August 1988

Dedicated to my parents

Ram Kishan

&

Shanti Devi

Name of the Candidate	-	Ashok Kumar Singal
Title of the thesis	-	Lunar occultation observations and a study of cosmic size evolution of extragalactic radio sources.
Degree	-	Ph.D.
Subject	-	Physics
Name of the Guiding Teacher	-	Prof. Govind Swarup
Institute	-	Tata Institute of Fundamental Research

STATEMENT REQUIRED UNDER ORDINANCES 0.770 AND 0.771

1) Statement required under 0.770:

The work presented in this thesis has not been submitted previously to the University of Bombay or to any other University for the award of Ph.D. or any other Degree.

2) Statement required under 0.771:

1. The work described in this thesis on the cosmic size evolution of extragalactic radio sources has been done entirely by me. The work presented in the thesis is original. The work has for the first time indicated that the luminosity size correlation among Radio Galaxies and Quasars is different and that the cosmic evolution of radio size may be different for the different radio luminosity classes.

2. The lunar occultation observations and analysis of 305 extragalactic radio sources described in this thesis were done by me jointly with Prof. M.N. Joshi, Dr. Gopal-Krishna and Dr. V.R. Venugopal. For the other data on extragalactic radio sources used in the study of their size evolution, appropriate references have been given in the text.

Ashok Kumar Singal

Ashok Kumar Singal

Certified that the above statements are true.

G. Swarup

Govind Swarup (Sr. Professor)

CONTENTS

LIST OF PUBLICATIONS

(1) Lunar occultation observations of 65 radio sources at 327 MHz : list 7
Ashok K. Singal, Gopal-Krishna and V. R. Venugopal
Mem. astr. Soc. India, 1, 14 (1979)

(2) Lunar occultation observations of 15 Abell clusters at 327 MHz
Ashok K. Singal, Gopal-Krishna and H. Steppe
Mon. Not. R. astr. Soc., 191, 581 (1980)

(3) Ooty lunar occultation survey : list 9
Mohan N. Joshi and Ashok K. singal
Mem. astr. Soc. India, 1, 49 (1980)

(4) The exceptionally large flux variability of the quasar 1055+018 at metre wavelengths
Gopal-Krishna, A. K. Singal and S. Krishnamohan
Astr. Astrophys., 140, L19 (1984)

(5) The alignment of distant radio sources
Vijay K. Kapahi, Ravi Subrahmanyan and Ashok K. Singal
Nature, 313, 463 (1985)

(6) Covariance of narrow-band noise in multiple beams of a phased-array system
Ashok K. Singal
IEEE Trans. Ant. Prop., Vol.AP-33, 455 (1985)

(7) Ultra-relativistic bulk motion and radio flux variability of active galactic nuclei
Ashok K. Singal and Gopal-Krishna
Mon. Not. R. astr. Soc., 215, 383 (1985)

(8) Magnetization effects in an incoherent synchrotron source

Ashok K. Singal

Astr. Astrophys., 155, 242 (1986)

(9) Some Corrections in the derivation of synchrotron radiation formulae

Ashok K. Singal

Astrophys. J., 310, 733 (1986)

(10) Polarization properties of radio cores in active galaxies

D. J. Saikia, Ashok K. Singal, T. J. Cornwell

Mon. Not. R. astr. Soc., 224, 379 (1987)

(11) Ooty lunar occultation survey of radio sources

A.K. Singal

Astr. Astrophys. Suppl. Ser., 69, 91 (1987)

(12) Cosmic evolution of the physical sizes of extragalactic radio sources and their luminosity-size correlation

Ashok K. Singal

Mon. Not. R. astr. Soc., 233, 87 (1988)

LIST OF FIGURES

LIST OF PLATES

LIST OF TABLES

SYNOPSIS

Right in the early years of radio astronomy, it was realized that the population of extragalactic radio sources consists of extremely powerful sources, which should be visible even at large cosmological distances. It was hoped that by using these sources as deep probes into the Universe we may be able to decide between the various cosmological world-models and thus perhaps unravel some of the mysteries of the Cosmos. The subsequent studies have shown that the population of extragalactic radio sources evolves heavily with the cosmic epoch and that the evolution almost completely masks out any distinguishable features of the geometry among various world-models. But a study of the cosmic evolution of various properties of these radio sources may still yield valuable information on the conditions which prevailed in the Cosmos at different epochs. Physical size of the population of extragalactic radio sources is one such property. The cosmic evolution of physical size of extragalactic radio sources has been examined in the past either by making a direct comparison of the observed angular size distribution with redshift or from an analysis of the variation of angular size with flux density. Both these kind of studies have shown the inadequacies of constant physical size models for the population of extragalactic radio sources and the inference has been that there is an evolution in physical size in the sense that the sources had smaller physical sizes at earlier epochs. But a suitable luminosity-size correlation among the radio source population could also explain these observations, without invoking any size-evolution.

In the present work we have investigated the problem of size evolution of extragalactic radio sources by examining their size distribution in the luminosity-redshift plane. In this way not only do we figure out the presence of any size evolution with redshift which may be present in various luminosity classes, but we also come to know of the existence of any luminosity-size correlation at various redshifts. In fact there are indications in our study that both the size evolution and the luminosity size correlation may be different among radio galaxies and quasars, and accordingly we have studied these two optical classes separately. For our purpose we need information on the flux density, angular size, optical class and redshift for each source in our sample. We have observed a large sample of ~ 300 extragalactic radio sources with the Ooty Radio Telescope at 327 MHz, using the lunar occultation technique. In addition to the information on flux density, a reliable estimate of the largest angular size of the observed radio source is also possible from the occultation technique, which provides arcsec resolutions, although along a few one-dimensional scans only. Moreover the arcsec accuracies of radio positions obtained from occultations, make it possible to get reliable optical identifications, allowing us to classify these sources into galaxies and quasars, and also leading to estimates of their redshifts, at least for the galaxies.

In chapter 1 we describe main features of the Ooty Radio Telescope (ORT). As the ORT beams have a sharper response in the north-south direction, the pointing also needs to be more accurate in that direction. The pointing of ORT in north-south is done electronically, by using a discrete set of RF and IF phase-shifters. In chapter 1 we discuss a procedure for eliminating some of the discontinuous steps which appear in the RF pointing of ORT in north-south, because of the discrete nature of these phase shifters. Refraction effects due to the troposphere, and partly due to the ionosphere, shift the ORT beams almost off source when the observations are carried out near horizon. Actually the ORT is a phased array system in the north-south, and as such a horizontally stratified plane parallel atmosphere should give rise to no refraction effects for such a system. But mainly due to the fact that the ORT has an incline of 11°.5 in north-south, added to the effects of a curved atmosphere, make the pointing errors due to refraction appreciable. In chapter 1, we have discussed these refraction effects on the pointing of ORT. Recently ORT has been converted into an aperture synthesis system by putting many smaller antennas at some appropriate locations. While discussing the refractions effects, we have also cosidered the pointing of OSRT (Ooty Synthesis Radio Telescope).

By using different phase gradients across ORT, which is a phased array system in north-south, a set of 12 simultaneous beams has been formed in north-south. During observations with the ORT, often a source may not be lying exactly on the maxima of any specific beam and accordingly the signal may appear simultaneously within 2 or more neighbouring beams. In such a case it is tempting to combine the simultaneous response in various beams to get a better signal to noise ratio. But such an improvement depends upon the temporal correlation of noise among these beams. In chapter 2 we have discussed this problem and have shown analytically that the noise correlation among two neighbouring beams, formed from the same elements in a phased array system, as a function of the angle of separation of these beams is the same as the individual beam pattern. The result is almost independent of the way the beams are formed. Actual comparisons of the observed noise correlation among various beams of ORT as a function of their angle of separation, with the beam pattern, both for the total power beams and the correlation beams, are made.

Some details of the lunar occultation technique, the method of observations and the data analysis procedure are discussed in Chapter 3.

Data analysis procedure includes the radio position determination, optical identification, angular size determination and the flux determination for the whole source as well as for the individual components, whenever multiple discrete components are seen. Chapter 3 also contains the tabulated radio and optical data on ~ 300 occultation sources observed by us with the ORT. Finding charts for 66 newly identified optical cases are also given. Additional notes and comments on some individual sources are also included in the text.

The cosmic evolution of physical size and the luminosity-size correlation for the population of extragalactic radio sources are investigated in Chapter 4. It is argued that in order to make these investigations, an extensive data base covering a large range of radio flux density, is needed. For this purpose we have supplemented our Ooty occultation source sample with many sub-samples, selected from the literature, at various flux levels. All the sources in our thus formed sample are optically identified, and their redshifts are either known from spectroscopic measurements or are estimated from optical magnitudes. Radio spectral data for most of these sources is also available. Thus for all these sources we can calculate the radio luminosity and the physical size for any given world-model. By using this large sample of 669 sources we have examined their physical size distributions in different luminosity-redshift bins, separately for galaxies and quasars. It appears that for radio galaxies the physical size increases with luminosity for redshifts $\lesssim 0.5$, where reliable data are available. Moreover it is found that the physical size decreases with increasing redshift for the radio galaxies with luminosity $10^{26} < P_{408} < 10^{27}$ W/Hz, where the median value of largest linear dimension drops from ~ 300 kpc for nearby sources to ~ 100 kpc at redshifts ~ 0.5. This drop in size can be represented by the size evolutionary models of type $(1+z)^{-n}$, for $n \approx 3$. The observed size evolution can also be fairly well described by other models including one in which there is an exponential increase in the physical size of radio sources with the cosmic time. For brighter radio galaxies ($P_{408} > 10^{27}$ W/Hz), there is little evidence for size evolution, at least upto redshift ~ 0.5; at higher redshifts data are lacking mainly because of the incompleteness of optical identification.

For quasars, unlike galaxies, there is no evidence of an increase in size with luminosity; in fact there is a hint of an inverse correlation between luminosity and size. Only a marginal size evolution seems to be present for different luminosity classes among quasars. The possibility of a differential size evolution for different luminosity classes among galaxies and/or that of an intrinsic difference in the size distribution among galaxies and quasars can not be ruled out.

CHAPTER 1

OOTY RADIO TELESCOPE

Ooty Radio Telescope (ORT) is an astronomical instrument designed primarily for the Lunar Occultation (LO) observations of radio sources. It is in the shape of a parabolic cylinderical reflector with a length of 529 metres along north-south, and a cross-section of 30 metres along east-west. The reflecting surface is made up of about 1100 stainless steel wires, stretched lengthwise along the north-south direction. The reflecting surface is illuminated by 1056 half-wave dipoles placed along its north-south focal line; these dipoles are grouped into 22 modules of 48 dipoles each. The voltage signals from each of these modules are divided into 12 parts and are then appropriately combined together to form 12 simultaneous neighbouring beams, separated by 3 secδ arcmin in declination. Each of these beams can be operated simultaneously, in the total power mode where the voltage signal from all the 22 modules are added together and passed through a square law detector, and in the correlator mode where the combined output of 11 north modules is multiplied with the combined output of 11 south modules.

The ORT has an equatorial mount with its north-south axis made parallel to the axis of earth by laying it along a natural hill whose north-south slope is equal to the local latitude of the place. The system is made mechanically steerable in hour angle about this axis, while in declination the set of 12 simultaneous beams can be steered by generating an appropriate phase gradient across the ORT cylinder in the north-south direction. The system is thus made steerable mechanically between $-4^h\ 07^m$ and $+5^h\ 20^m$ in hour angle and electronically from $-36°$ to $+36°$ in declination. The system operates at a frequency of 326.5 MHz with a 4 MHz bandwidth.

The details of the mechanical structure and the receiver system have been described by Swarup et al.(1971) and Sarma et al.(1975). Kapahi et al.(1975) have described the feed system at the focal line. The mechanical phase shifters as described by Kapahi et al.(1975) have since then been replaced by the new diode phase shifters (Joshi et al. 1988). Very fast steering in north-south is now possible with the help of diode phase shifters under computer control.

The ORT beams have a full half-power width of about $2.^{\circ}3$ in right ascension, and of 5.6 secδ and 3.6 secδ arcmin in declination for the total power system and the correlator system respectively. It is obvious that the pointing has to be more accurate in north-south. In this chapter we discuss some aspects of the pointing of ORT, mainly concentrating on the declination pointing. The various aspects discussed are: (i) the broad scheme of declination pointing (Section 1.1) (ii) the discreteness in the beam pointing due to finite steps in the phase gradient (Section 1.2). (iii) Effects of refraction on the pointing (Section 1.3). Recently ORT has been made part of an aperture synthesis system called the Ooty Synthesis Radio Telescope (OSRT), by putting a large number of smaller parabolic cylinders at suitable locations around ORT (Swarup 1984). In Section 1.3 we shall briefly discuss the refraction effects for the OSRT system also.

1.1 BROAD SCHEME OF THE POINTING OF ORT IN DECLINATION:

ORT, as far as its pointing in declination is concerned, is a phased array of 22 modules, each module in turn being a phased array of 48 dipoles. All the modules, as well as the dipoles within each module, are spaced uniformly along the north-south direction. Because the north-south axis is made parallel to the axis of earth, the radio waves coming from the direction of 0° declination arrive simultaneously at all the array elements. But the radio waves coming from a direction $\delta°$ arrive with a progressive time delay $d \sin\delta/c$ between successive elements, d being the distance between two adjacent elements. This gives rise to a phase difference $\phi = 2\pi d\, \nu \sin\delta/c$, between successive elements (fig. 1.1) at a frequency ν.

In order to phase the array in direction δ, we have to compensate for the above phase difference by providing extra path lengths through cables for the successive elements in the reverse order. The phase ϕ as calculated above, in general, consists of n integer cycles (of 2π radians each) and a proper phase (fraction of a cycle). If we were to compensate only for the proper phase at a given frequency, then the integer cycles would leave a large residual phase for the other frequency components in the band to broaden the beam excessively. For the ORT, all dipoles within each module are phased towards the intended direction at RF stage itself using the diode phase shifters (Joshi et al. 1988). Further the phase differences between individual modules are taken care of at the IF stage through appropriate cable lengths. It is at the IF stage where large cable-lengths are introduced to compensate for the time delays in steps of integer cycles, thus maintaining the signal coherence among various modules. The available lengths of cables presently allow the steering to be done in the range of ±36° in declination.

1.2 DISCRETE STEPS IN THE PRIMARY-BEAM POINTING

The discrete nature of the phase-shifters employed for the RF system of ORT gives rise to discrete steps in its primary-beam pointing in the

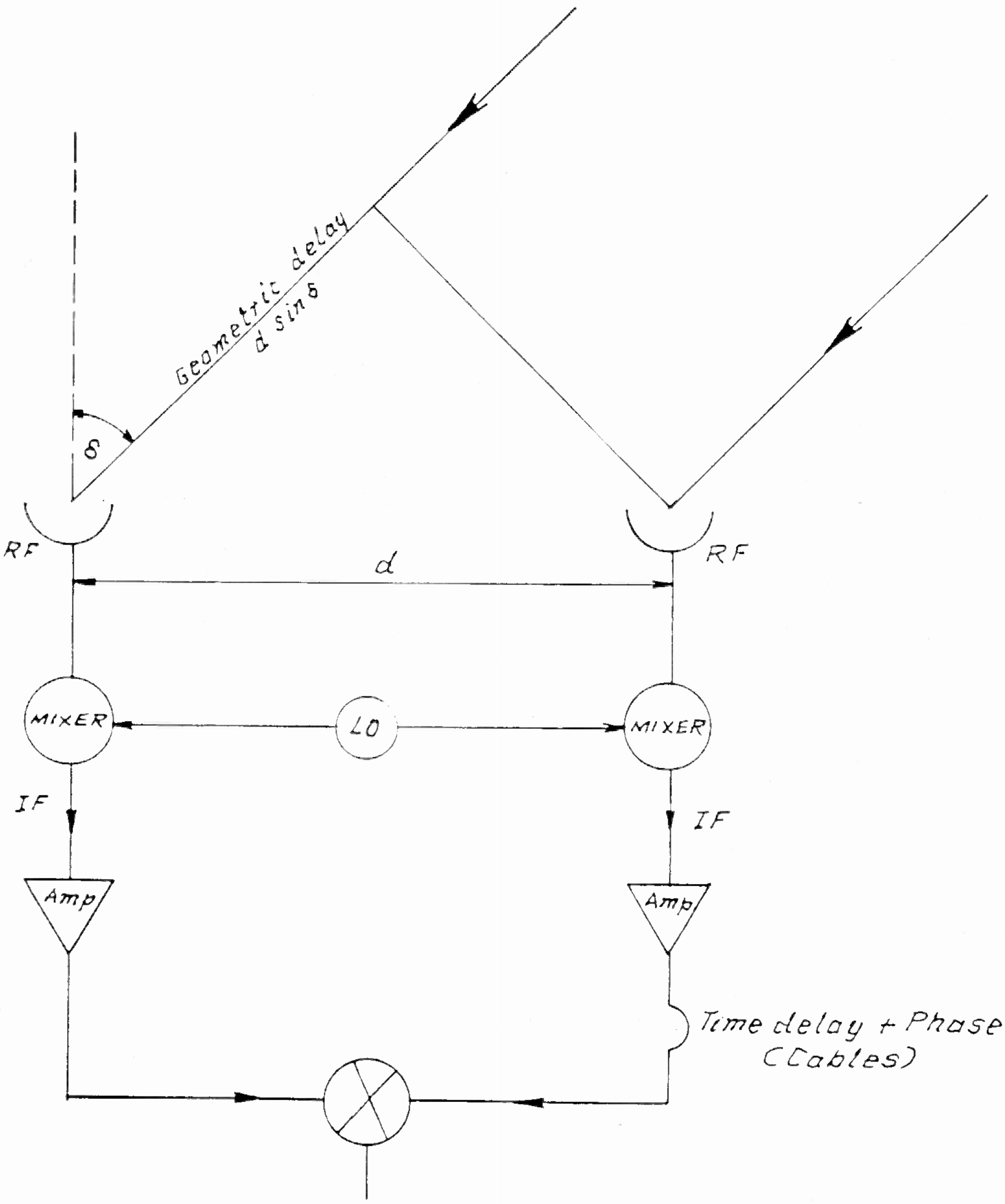

Fig 1.1 A schematic of the declination setting system of the ORT

north-south direction. Here we discuss this effect and a procedure to eliminate these steps.

As discussed earlier the ORT in the north-south direction consists of 22 modules, each of 23 metres in length. Each module consists of 48 dipoles, with 24 dipoles on either side of its centre. The distance between successive dipoles is accordingly given by

$$d = \frac{23^{m}.0}{48} = 0^{m}.4792 = 0.5219\ \lambda_{RF}\ , \quad \text{where } \lambda_{RF} = 0^{m}.9182$$

The pointing of ORT in north-south is done by generating an appropriate phase-gradient. For this, first the individual modules are aligned towards the intended direction by putting a proper phase distribution at RF stage for the dipoles, we call it the 'primary-beam pointing' of ORT. The phase difference between successive modules is adjusted at IF stage.

The digital phase-shifter system for primary-beam pointing of ORT employs 4 bits for each dipole, wherein the phase distributions for individual dipoles can be changed only in discrete steps of $2\pi/2^4 = 2\pi/16$ radians. In the usual approach, one calculates the required phase distribution for each dipole and rounds it off to the nearest integer multiple of $2\pi/16$ for setting the bits. The phase distribution for dipoles on one side of the centre of a module is exactly antisymmetric to that for dipoles on the other side, hence we shall concentrate in our discussion on the phase distribution for mainly on one side of the module. Discrete steps in the phase distribution put a restriction on the minimum discrete steps allowed in the pointing of ORT for certain directions. For example, starting northwards from 0° declination, where there is a zero phase-gradient across the module, the first LSB (least significant bit corresponding to a phase value of $2\pi/16$) in the extreme dipole gets set only at a minimum declination given by

$$2\pi(24-\frac{1}{2})\ 0.5219 \sin\delta_1 = \frac{2\pi}{16}\cdot\frac{1}{2}$$

$$\Rightarrow \delta_1 \sim 8'.76$$

Thus for all the intended settings between -8'.76 to +8'.76, there is no change in the phase distribution within the module, and the pointing is essentially towards 0° declination. The next change in pointing occurs when LSB is set also in the last but one dipole. This is when

$$2\pi(23-\frac{1}{2})\ 0.5219 \sin\delta_2 = \frac{2\pi}{16}\cdot\frac{1}{2}$$

$$\Rightarrow \delta_2 \sim 9'.15$$

This step of 0'.39 (=9'.15-8'.76) is quite small as compared with the first one of 8'.76, starting from 0° declination. Similarly the other next steps can be calculated. In general, successive steps between two consequtive settings will be small except near certain directions. These certain 'troublesome' directions are those for which the phase distribution is such that the adjacent dipoles differ in phase by integer multiples of $2\pi/16$. In case of even integer multiples, one will get the ideal setting with phase difference between successive dipoles exactly compensated for. But for odd integer multiples, all 24 dipoles on one side of the centre of module will have a constant phase error of $+2\pi/32$ while the remaining 24 dipoles on the other side will have a constant phase error of $-2\pi/32$. But in all cases of integar multiples there will be large discrete steps of size = ±8'.76 secδ in the pointing. These 'troublesome' directions are thus given by

$$2\pi\ 0.5219 \sin\delta = \frac{2\pi n}{16}, \quad \text{where n is an integer.}$$

Accordingly it appears that in the usual approach, large steps in primary-beam pointing occur around declinations, $\delta=0°$, $\pm 6°.88$, $\pm 13°.86$, $\pm 21°.06$, $\pm 28°.62$ etc.

1.2.1 Optimum Direction Of Pointing

Apart from these large apparent discrete steps in pointing, in the above usual approach for calculating phase distribution, the pointing itself may not be very satisfactory. To see this let us calculate where the beam is 'actually' pointing at when, for example, for the intended pointing direction of $\delta \sim 9'$, we in the usual scheme, put $\pm 2\pi/16$ phase in the extreme dipoles. To find the 'actual' pointing direction we can use the least square error method of the 'Fitted Straight Line' on the similar lines as described by Hatcher(1973). We outline this method in the following way:

First, let us enumerate the dipoles within a module with an index $i=1$ to N, where $N=24$ in our case; as mentioned earlier we concentrate only on dipoles on one side of the module and for these we shall measure the phase difference with respect to the centre of the module. Let ϕ_i denote the actual phase put for the ith dipole for a given setting. For a pointing towards direction δ, ith dipole would have ideally a phase value, $\phi_i'=2\pi d \sin\delta\,(i-1/2)/\lambda$, where d is the distance between two adjacent dipoles. Now we form a quantity $S_\phi = \sum(\phi_i-\phi_i')^2$. For the given phase distributions ϕ_i, S_ϕ will be a function of $\sin\delta$. We define that value of δ to be the 'actual' pointing direction for which S_ϕ is a minimum. If we write $\phi_i'=\phi_0(i-1/2)$, where $\phi_0=2\pi d/\lambda \sin\delta$, then minimizing S_ϕ with respect to ϕ_0, we get

$$\frac{\partial S_\phi}{\partial \phi_0} = \sum_{i=1}^{N} (\phi_i'-\phi_i)\,(2i-1) = 0$$

or

$$\frac{\phi_0}{2} \sum_{i=1}^{N} (2i-1)^2 = \sum_{i=1}^{N} \phi_i \, (2i-1) .$$

Using the series $\displaystyle\sum_{i=1}^{N} (2i-1)^2 = \frac{N(2N-1)(2N+1)}{3}$,

we get $$\frac{\phi_0}{6} N(2N-1)(2N+1) = \sum_{i=1}^{N} \phi_i \, (2i-1)$$

or

$$\phi_0 = \frac{6}{N(2N-1)(2N+1)} \sum_{i=1}^{N} \phi_i \, (2i-1) .$$

This allows us to calculate the 'actual' direction of pointing in the least-mean-square sense for any given phase distribution ϕ_i.

From this we can readily calculate that for the intended pointing towards direction $\delta \sim 9'.0$, when in the usual scheme only the 24th dipole has a phase of $2\pi/16$, the 'actual' pointing of the primary-beam is towards $\delta \sim 2'.1$, and for the intended pointing towards, say, $\delta \sim 9'.2$, when both the 23rd and the 24th dipoles have $2\pi/16$ phase each, the actual pointing of the primary-beam is towards $\delta \sim 4'.1$ and so on. Thus there could be substantial pointing errors in the usual scheme, but again it should be noted that these errors become significant only around the above mentioned 'troublesome' directions.

1.2.2 A Scheme To Eliminate Large Steps

We have shown above how to estimate an optimum direction of pointing for a given phase-distribution. But our problem really is the other way, we need some simple scheme to calculate an optimum phase distribution ϕ_i, for an intended direction of pointing . In case of manual operations, such schemes really may not be very practical,but if the phase-bits setting is done under computer control, we can employ the following scheme:

First we compute the actual required phase values, ϕ_i', for the intended direction, δ_0, and then round off these values to the nearest integer multiple of $2\pi/16$ to get ϕ_i in the usual way. Then we also calculate $\Delta\phi_i=\phi_i-\phi_i'$, for all i and form the sum $E_\phi = \sum(\Delta\phi_i)(2i-1)$. If E_ϕ turns out to be zero, then this setting itself gives the 'actual' pointing towards δ_0. But if E_ϕ is finite, then we can adjust the phase values ϕ_i in such a way as to make E_ϕ as small as possible. Then for these ϕ_i values, the optimum direction, as calculated in section 1.2.1, will be as near to the intended direction δ_0, as possible with the discrete phase distributions.

While adjusting ϕ_i values to make $E_\phi = \sum (\Delta\phi_i)(2i-1) \longrightarrow 0$, one needs caution. An important aspect of the problem, in fact ignored by Hatcher(1973), is that, while it is true that the procedure described in section 1.2.1, gives an optimum pointing direction for the given phase distribution, but it does not imply that the given phase distribution is the optimum one for the pointing in that direction. In fact, the condition $\sum(\Delta\phi_i)(2i-1) = 0$ could be satisfied for a variety of contrived phase distributions to give the same 'actual' pointing direction. For example, even for the 'actual' pointing towards $\delta=0°$, one could put large phase jumps across the module but still satisfy $E_\phi = 0$. All such unrealistic phase distributions will give rise to large side-lobes and decrease the beam efficiency. Of course for any of such phase distributions the principal maxima of beam would still be pointing towards $\delta=0°$. Thus while adjusting ϕ_i values, one has to act judiciously.

We describe here a simple and efficient procedure, which meets the above requirements and is quite fast in execution.

We put the corrections, in the form of discrete phase of value $\pm 2\pi/16$, starting from the dipole having largest absolute value of $\Delta\phi$, and then recalculate E_ϕ after this correction. If absolute value of E_ϕ decreases due to this correction then one goes to the next largest value of $\Delta\phi$ for correction and so on. At any stage when absolute value of 'corrected' E_ϕ is larger than the just previous one, one quits the loop and also revokes the last made correction.

In this way one does not 'over correct' the individual phases and mostly the corrections are done only for largest errors, thus also minimizing the total number of corrections to be made. It should be noted that in this way no dipole could be in error from the required exact phase by more that the smallest discrete step, i.e., $2\pi/16$. Implementation of this procedure is quite simple, ofcourse first all the optimum phases to be put are calculated and only then the bit patterns are set in a single go.

In this procedure, starting from $\delta=0°$, the first LSB in the 24th dipole gets set at a declination value of 1.'05 and remains so till 3'.05, after which the LSB in the 23th dipoles also gets set and thus it goes on. This procedure not only gets rid of the apparant discrete steps in the pointing but also sets the phase distributions in an optimum way.

This procedure has effect mainly near the 'troublesome' directions; for other directions, errors $\Delta\phi_i$ are in any case small in the usual procedure itself.

Figs. 1.2 and 1.3 show the testing of the above procedure using ORT.

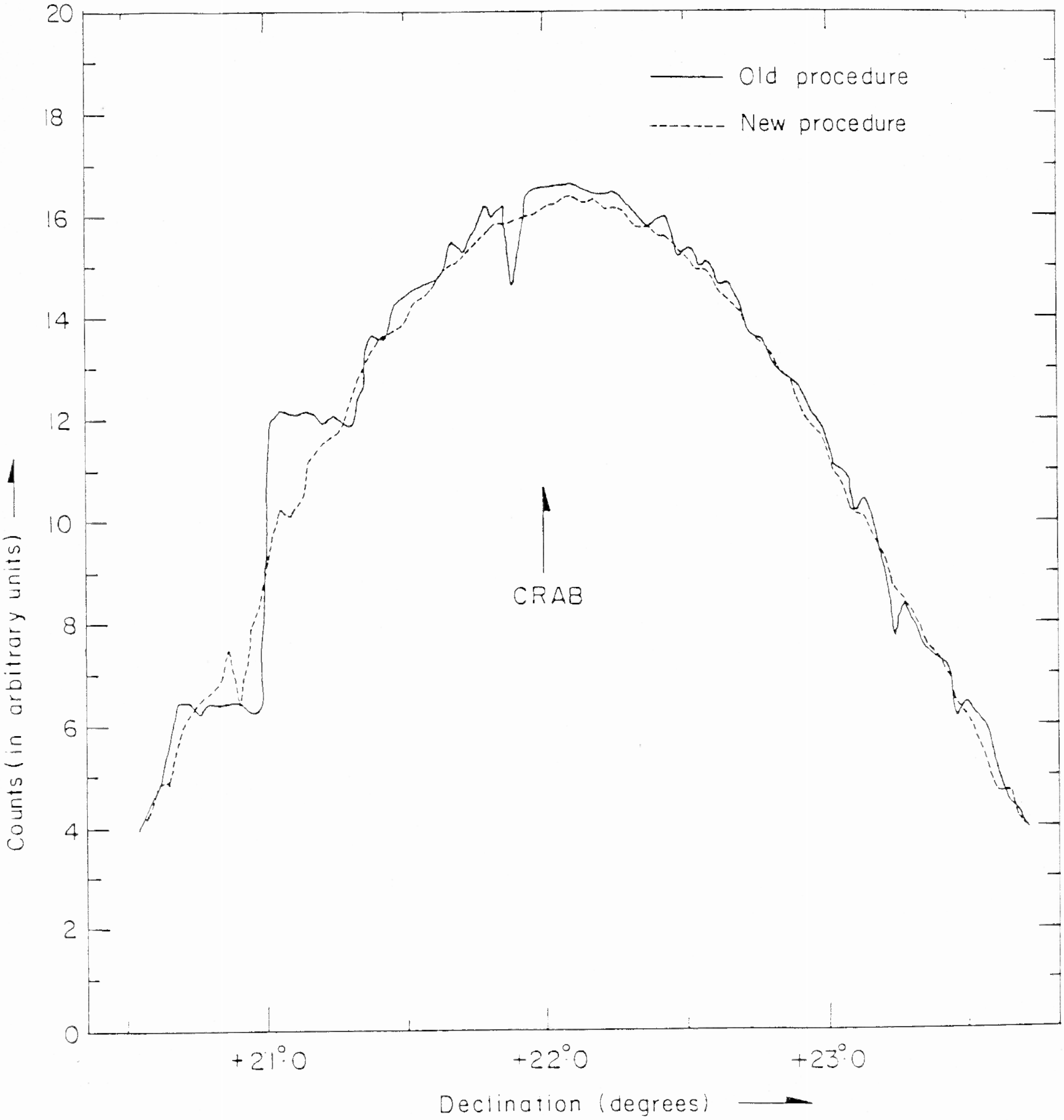

Fig 1.2 A comparison of the new and old procedure for the primary beam pointing using CRAB

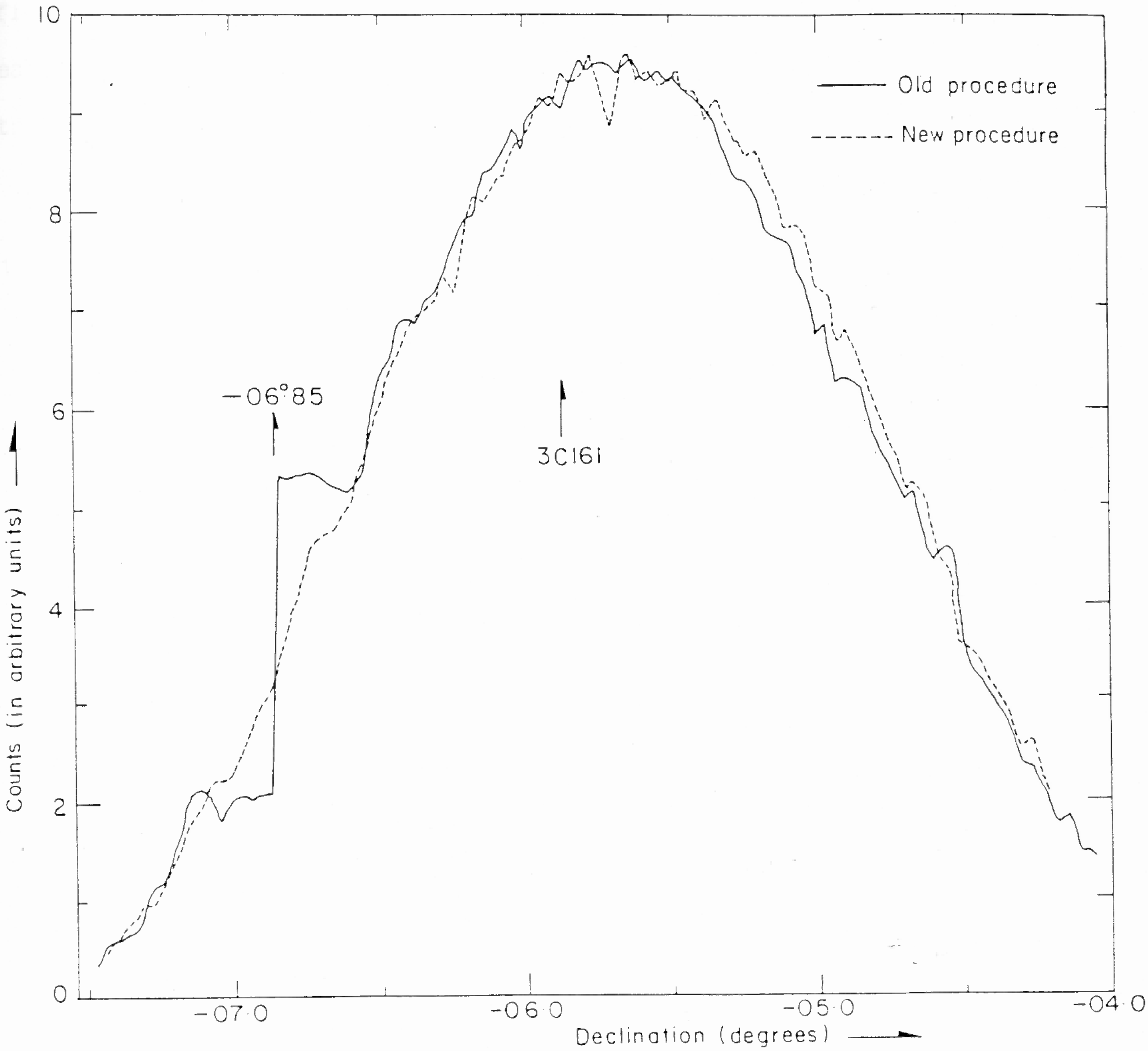

Fig 1.3 A comparison of the new and old procedure for the primary beam pointing using 3C161

A strong source, unresolved with the primary-beam , was scanned in north south using only the RF phase shifters. The observations were made using both the usual procedure and the proposed new procedure. The improvement in pointing with the new procedure is very obvious from the figs. 1.2 and 1.3. The observations were made for Crab and for 3C161, in each case the broad plateau (around $\delta=+21'.06$ and $\delta=-6'.88$ respectively) in the usual procedure gets replaced by a smooth curve in the new procedure.

1.3 REFRACTION EFFECTS ON THE POINTING OF ORT AND OSRT

Here we shall consider the refraction effects of only an average troposphere and ionosphere. Effects of the irregularities either in the troposphere or in the ionosphere, which in any case are highly time variable, will not be considered here.

1.3.1 Refraction Effects Of The Troposphere:

First we shall consider a horizontally stratified parallel plane atmosphere. In this case, the normal bending of a wavefront, important for a single dish observations, has no effect for an interferometer system lying in a horizontal plane. This can be seen in the following way.

Let the source be lying at a true zenith angle z as seen from the top of the atmosphere, i.e, without the refraction effects. As the rays enter the atmosphere, due to refraction the rays will appear to come from a zenith angle z', given by $\mu \sin z' = \sin z$. The wave front which was at an angle z with respect to the horizontal plane will now be at an angle z' (fig.1.4). So an individual single dish will have to point towards the

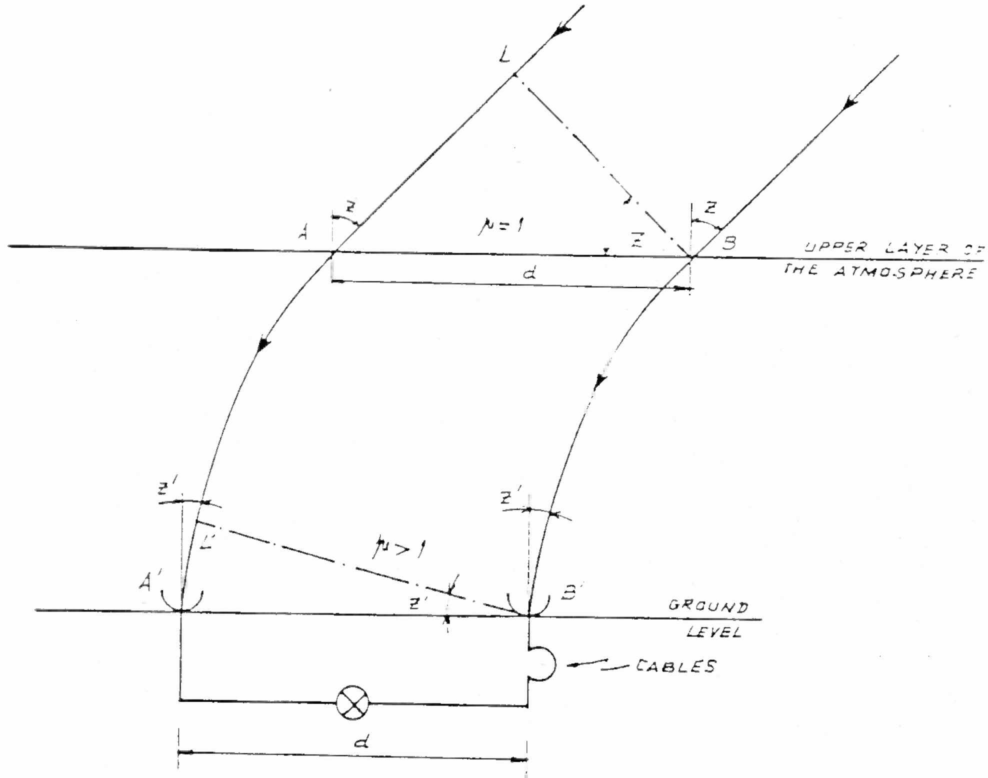

Fig 1.4 Geometry of tropospheric refraction for an interferometer system lying in a horizontal plane

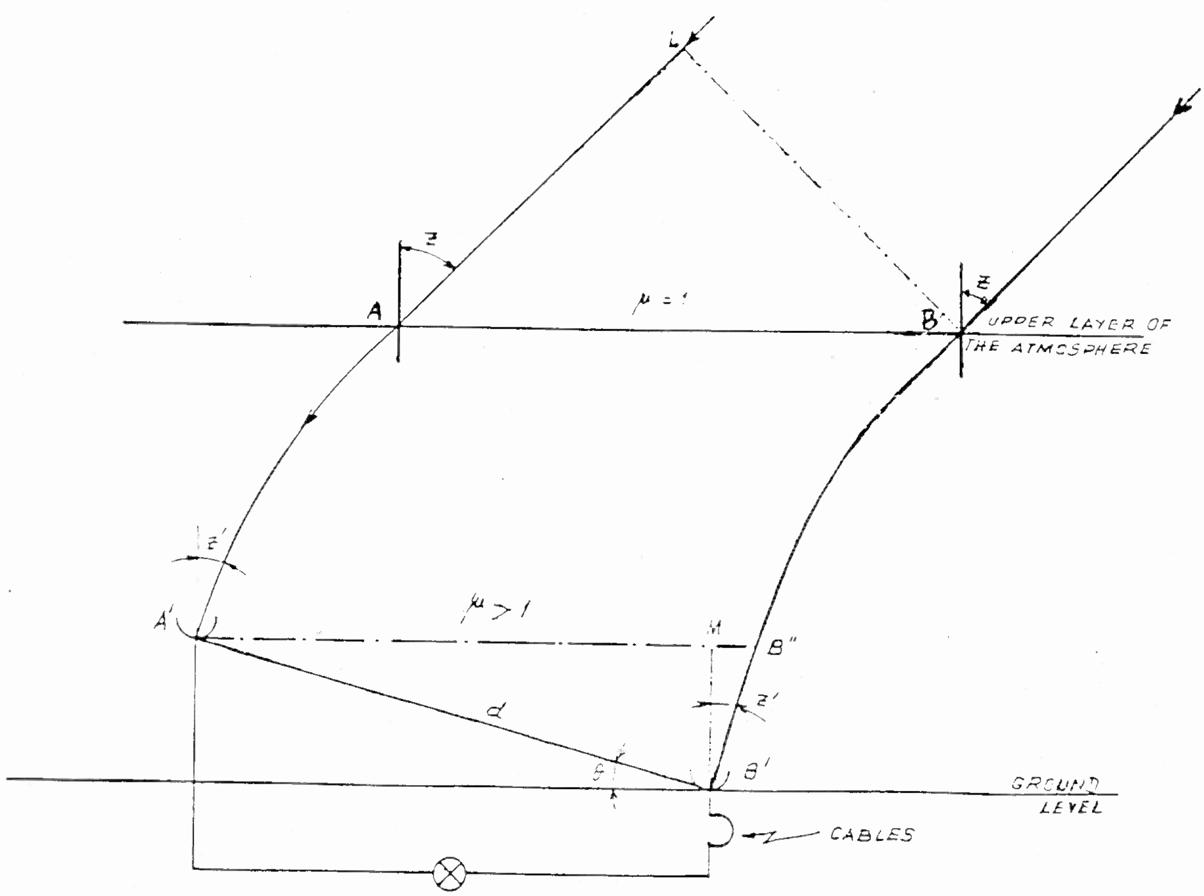

Fig 1.5 Geometry of tropospheric refraction for an interferometer system, inclined to the horizontal plane

apparent zenith angle z' instead of the true zenith angle z. But for an interferometer it can be seen easily that the phase difference between A' and B' is the same as it was between A and B ($\because$ AA'=BB'). This can be seen in another way: let ϕ be the phase difference between A and B, and ϕ' be the phase difference between A' and B'. Then the change in phase

$$\phi'-\phi = \frac{2\pi}{\lambda}(\mu\, A'L' - AL)$$

$$= \frac{2\pi d}{\lambda}(\mu \sin z' - \sin z) \quad \ldots \quad (AB=A'B'=d)$$

$$= 0$$

Thus if we are going to compensate for the phase difference between A' and B' by using cables in the path of signal from B' (or A'), the length of these cables is independent of the refractive index of the atmosphere, because the final phase difference is the same as it was between A and B. This statement is true even if the refractive index changes with height and the bending of rays takes place continuously. We will be putting the cable lengths as if the source were at a zenith angle z and there were no refraction present. Thus the bending of wavefront due to refraction has no effect on the pointing of an interferometer system lying in a horizontal plane. It should be noted that the above statement is true even if the source does not lie in the vertical plane passing through A'B'. For example if A' and B' lie on a north-south line, then for any hour angle position of the source, the above statement will still hold true.

Let us consider now the case when our interferometer system is not lying in a horizontal plane but is inclined at an angle θ with respect to it (see fig. 1.5). Then the ray reaching B', as compared to the one reaching A', would have travelled an extra path

$$\mu B'B''-AL = \mu\, B'M \sec z' - AB \sin z$$

$$= \mu\ d \sin\theta \sec z' - A'B'' \sin z$$

$$= \mu\ d \sin\theta \sec z' - (d \cos\theta + d \sin\theta \tan z') \sin z$$

Now without accounting for the refraction we would have also put cable-lengths in path of B' corresponding to a path difference of $d \sin(z-\theta)$. Thus, we get a total path difference of

$$\mu d \sin\theta \sec z' - d(\cos\theta + \sin\theta \tan z') \sin z + d \sin(z-\theta)$$

$$= \mu d \sin\theta \sec z' - d \sin\theta (\tan z' \sin z + \cos z)$$

and using the fact that $\sin z = \mu \sin z'$,

the total path difference $= d \sin\theta (\mu \cos z' - \cos z)$.

This amounts to a phase difference $= \dfrac{2\pi d \sin\theta}{\lambda} (\mu \cos z' - \cos z)$.

This formula for the phase difference can be interpreted in a simple way: (i) Only the vertical component of the baseline, $d \sin\theta$, is responsible for the refraction effects, (ii) $d \sin\theta \cos z'$ is the projection of the vertical component of the baseline, $d \sin\theta$, along zenith angle z' of the rays, arriving with a wavelength λ/μ in the atmosphere, (iii) $2\pi d \sin\theta \cos z/\lambda$ is the calculated phase difference in absence of refraction which we would have compensated for through cables-lengths.

It can be seen easily that the above formulae is true even if the source does not lie in the vertical plane passing through A'B'. Moreover the formula remains true even if the refractive index changes with height (of course we assume that the change in refractive index is negligible over a height difference of $d \sin\theta$). What matter here are the final values of μ and z' and the initial value of z (see fig. 1.5).

The assumption of a horizontally stratified parallel plane atmosphere is quite good as long as the zenith angle of the point of observations is not very large. At large zenith angles the effect of the curvature of the atmosphere must be taken into account. For this purpose one could adopt a model of the atmosphere being in uniform concentric spherical shells around the surface of the earth, the refractive index changing as we go from one shell to another. Alternatively one could simply assume that the whole of the atmosphere is within a single homogeneous spherical shell of an appropriate scale height and with a sharp boundary. The quantities of our interest in any of these models are the final direction of arrival of the rays and the values of the refractive index at the location of the antenna-elements. Of course, we assume that the refractive index value as well as the direction of arrival do not change from one interferometer element to another.

If baseline of length d extending from element A to elemnt B is characterised by an azimuth A_b and a zenith angle Z_b, and the apparent position of the source is given by an azimuth A_a and a zenith angle Z_a, then the projection of the baseline on the direction towards the source is given by (fig. 1.6)

$$d \cos \theta = d\,(\cos Z_a \cos Z_b + \operatorname{Sin} Z_a \operatorname{Sin} Z_b \cos (A_a - A_b)).$$

Now $d \cos \theta$ is the extra path for the ray reaching element A with respect to the one reaching element B, and the corresponding phase difference is given by

$$\frac{2\pi\mu d \cos \theta}{\lambda} = \frac{2\pi\mu d}{\lambda} (\cos Z_a \cos Z_b + \operatorname{Sin} Z_a \operatorname{Sin} Z_b \cos (A_a - A_b)).$$

If the true azimuth and the true zenith angle of the source are A_0 and

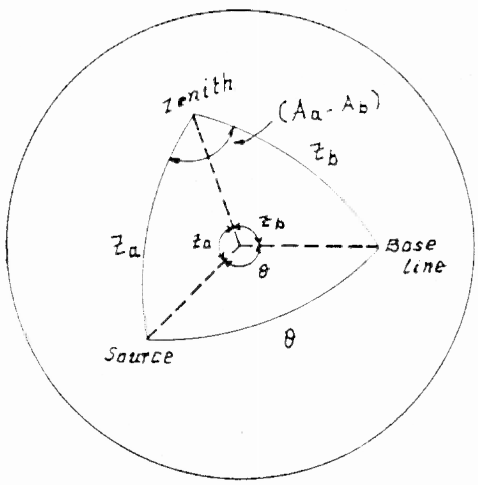

Fig 1.6 Geometry of the projection of the baseline on the direction towards source

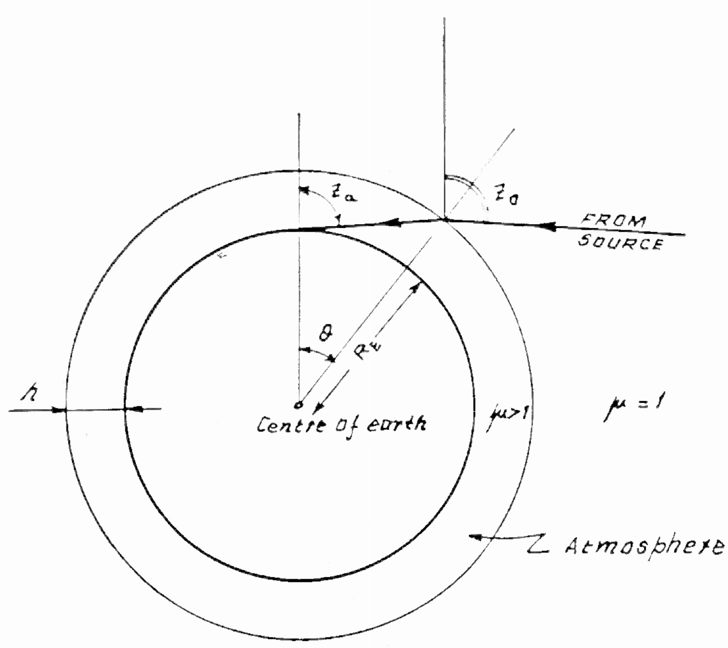

Fig 1.7 Relation between Z_a and Z_o for a single spherical shell model atmosphere

Z_0 respecively, then without the refraction effects, the phase difference should be

$$\frac{2\pi d}{\lambda} \left(\cos Z_0 \cos Z_b + \sin Z_0 \sin Z_b \cos (A_0 - A_b)\right).$$

Now based on the reasonable assumption of the spherical symmetry of the atmosphere, the source azimuth does not change due to refraction, i.e., $A_a = A_0$. Thus all we have to know is Z_a as a function of Z_0 in order to take into account the refraction effects.

There are various formulae available in literature for calculating Z_a as a function of Z_0 depending upon the chosen model for the atmosphere. For example, for a single homogeneous spherical shell model atmosphere with a uniform refractive index, Z_a and Z_0 are related by (fig. 1.7)

$$\mu \sin (Z_a - \theta) = \sin (Z_0 - \theta)$$

and

$$\sin (Z_a - \theta) = \frac{\sin Z_a}{1 + h/R_E}$$

Where h is the total assumed height of the atmosphere above the surface of earth, R_E is the radius of earth, and θ is the angle at the centre of the earth between the direction towards the observer and the point where the ray enters the atmosphere.

The other formulae, which account for the change in refractive index as a function of height, cannot be rigorously applied unless one has a precise knowledge of the relation between height and refractive index (Smart 1977). So various approximations and simplifying assumptions are made to derive usable formulae. But almost all such formulae including the ones given above for the single homogeneous spherical shell model fail, many giving almost absurd results, for high zenith angles ($z \geq 80°$).

In optical astronomy, Refraction-Tables since long are being used for large zenith angles. These tables are based on the actual observational data and these list refraction angle, $R=Z_0-Z_a$, as a function of Z_a or Z_0. We do not have such extensive refraction-tables available for direct use at radio frequencies and we have already mentioned that the various formulae are not very satisfactory at high zenith angles. A compromise could be arrived at by the use of appropriate formulae for low zenith angles, say for $z \lesssim 80°$, and using the modified optical refraction-tables for higher zenith angles. We know that for small zenith angles refraction angle, R, is directly proportional to μ-1. And we can except that even for large zenith angles the principal term will be proprotional to μ-1. In fact this will be the first order term in Taylor's series expansion of R, in terms of μ-1; the co-effecient of this term will be highly dependent on zenith angle. Zeroth order terms should obviously be zero, as there can be no refraction if μ-1=0. So we could simply multiply the value of R in refraction tables by a scaling factor given by $(\mu_{radio}-1)/(\mu_{optical}-1)$, and use that value for high zenith angles, This procedure appears very much justified from the refraction angle (=bending) versus surface radio refractivity data given Crane (1976) for a zenith angle of 85°. He also gives a procedure for the computation of refraction angle as a function of μ-1 at high zenith angles. In fig. 1.8 we have plotted refraction angle vs. true zenith angle from the tabulated values given by Allen (1973). Also plotted are the values obtained from Table II of Crane (1976) for the corresponding value of $\mu-1=290\times10^{-6}$. The match between these two independent sets of data, one from optical and the other from radio measurements, is so well that we can say there is essentially no difference between the two. We propose to use interpolated values from this plot for the refraction angle at high zenith angles.

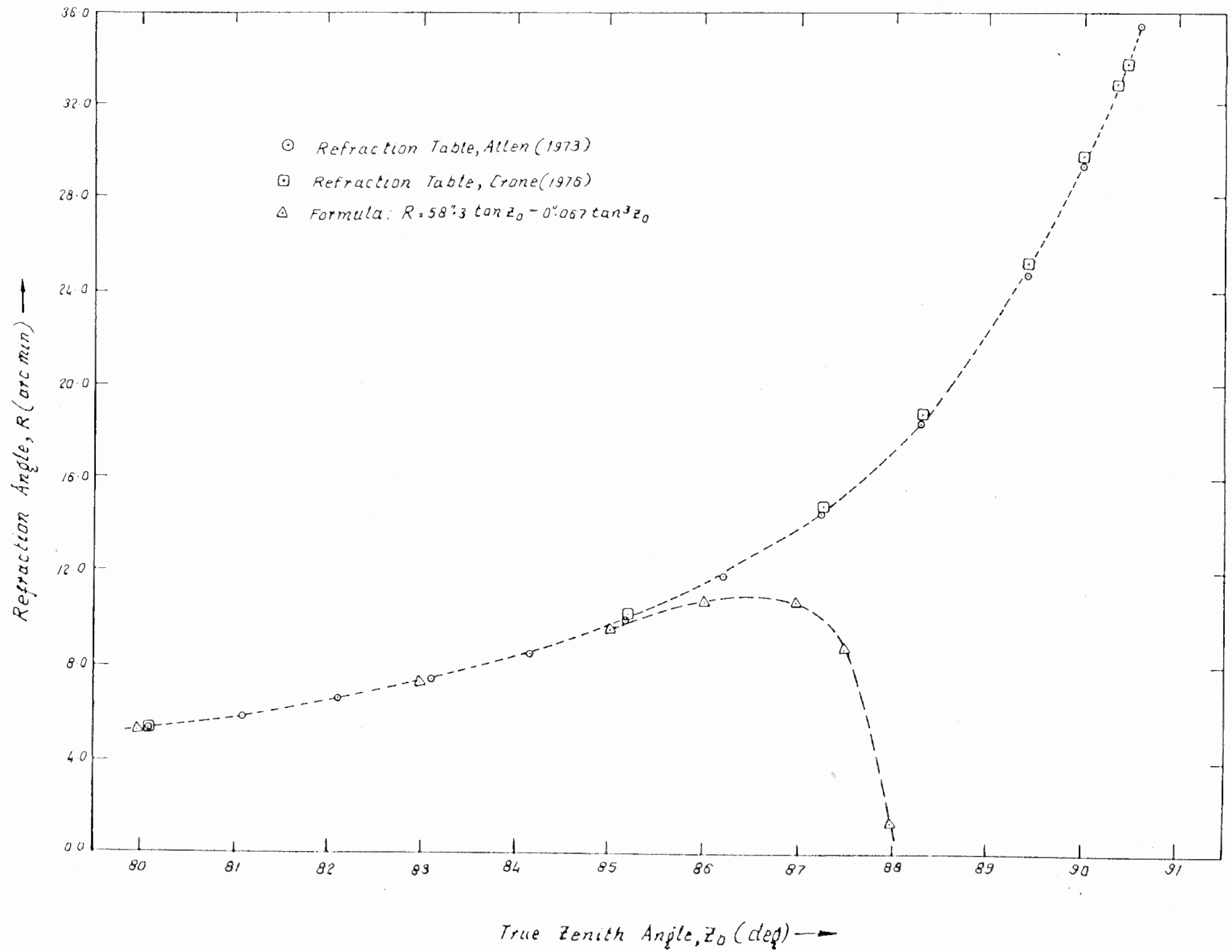

Fig 1.8 Tropospheric Refraction as a fuction of zenith angle

We use an average value of refractive index given by $\mu-1=250\times10^{-6}$, for application to ORT and OSRT; error in this value is unlikely to be much greater than 10% (Mathur and Sukumar 1976). Thus to convert for our use the refractive index values from the plot, we shall use a scaling factor of 250/290~0.86. For smaller zenith angles ($z_0<80°$) we use the formula (Allen 1973),

$R = A \tan Z_0 - B \tan Z_0^3$, where A=50".138, B=0".058 .

(These values have already been scaled down by a factor of 0.86)

A few values obtained from this formula for $Z_0 \geq 80°$ are also plotted in fig. 1.8 for comparison purposes. It is clear that while the above formula gives a very good approximation to the observational data up to $Z \leq 85°$, for higher zenith angles, this formula cannot be used.

1.3.2 Refraction Effects Of The Ionosphere

Bending due to the ionosphere refraction as compared with that due to the tropospheric refraction is much smaller at our frequency (326.5 MHz), ionospheric refraction being inversely proportional to $(\text{frequency})^2$. But it should be kept in mind that the ionosphere, due to its highly irregular behaviour, could produce highly variable refraction effects during the period of continuous observations, stretched over many hours. But here we consider only the average effects concerned with the pointing of various antennae.

Firstly, it should be noted that independent of the baseline orientation there should be no ionospheric refraction for a horizontally startified parallel plane ionosphere. Here we assume that the effects due to the horizontal gradient of electron density are negligible (Mathur and Sukumar 1976). Then it is only the spherical curvature of the ionosphere which produces bending of the rays. Thus we expect no change in the azimuth angle, only the apparent zenith angle will be different from the true zenith angle. To calculate it we need to know the value of refraction index as a function of height, which in turn requires the electron density profile as a function of height. From the electron density profile one can directly calculate the total bending using an expression like the one given by Hagfors (1976). In absence of that we simply adopt the plot of refraction bending vs zenith angle as given by Hagfors for an example electron density profile. We have scaled down the plot for our frequency (326.5 MHz) and also extrapolated the values below a zenith angle of 60° (fig. 1.9). Errors due to extrapolation cannot be larger than a few arcsec due to the low absolute value of bending in that region.

Though the refractive index value for the ionosphere is smaller than unity, the overall effect of bending is in the same direction as due to the troposphere, i.e., the apparent zenith angle is smaller than the true zenith angle. Thus the bending effects due to the ionosphere and due to the troposphere add up. In fact the apparent zenith angle, after the rays have entered and crossed the ionosphere, becomes the true zenith angle for the purpose of calculating the troposhperic bending. To account for the total refraction effects due to both the ionospheric and the tropospheric, we need to know the final apparent zenith angle at the location of antennae as a function of the true zenith angle above the ionosphere.

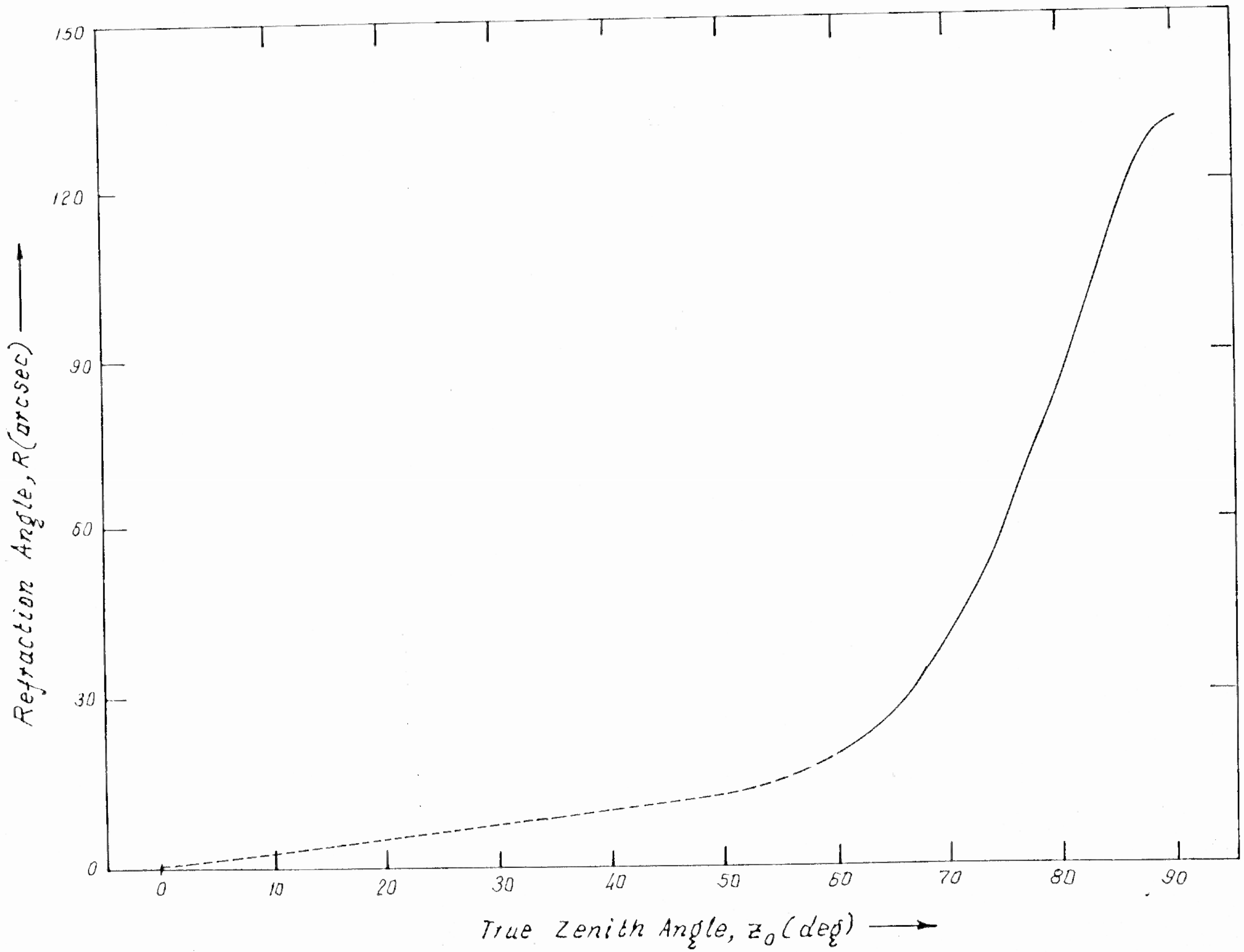

Fig 1.9 Ionospheric Refraction as a function of zenith angle

1.3.3 Application To ORT And OSRT

For ORT (as well as for the other smaller antennae), the east-west pointing is done purely by a mechanical rotation, thus the hour angle pointing will be directly affected by the bending due to refraction. We can calculate the apparent hour angle (H_a) of the source from its apparent zenith angle (Z_a) and the azimuth (A_o) by using the expression

$$\tan H_a = \frac{-\sin Z_a \sin A_o}{\cos \phi \cos Z_a - \sin \phi \sin Z_a \cos A_o}$$

Where $\phi(=11°23')$ is the latitude of ORT. Azimuth is measured eastwards from the north point. Fig. 1.10 shows the change in HA for different pointing directions, the maximum change for ORT is about 1^m.

ORT is a phased array system as for as its north-south pointing is concerned. The apparent declination (δ_a) is given by

$$\sin \delta_a = \sin \phi \cos Z_a + \cos \phi \sin Z_a \cos A_o$$

The appropriate phase-gradients across ORT in north-south can be calculated for the pointing towards δ_a, but it is necessary that the value of wavelength used for phase calculations should be λ_{vacuum}/μ, where μ is the refractive index value at the location of ORT. The same is true for the north-south pointing of all other individual antennae of OSRT.

West-side Story: It has been observed that when ORT is tracking a source for some continuous observations, then as the source approaches the west limit, its position shifts rapidly towards north with respect to ORT north-south beams. This shift, of the order of a few arcmin, causes the source to drift from one beam to another. This, so called 'west-side' story, can be easily explained in terms of the refraction effects.

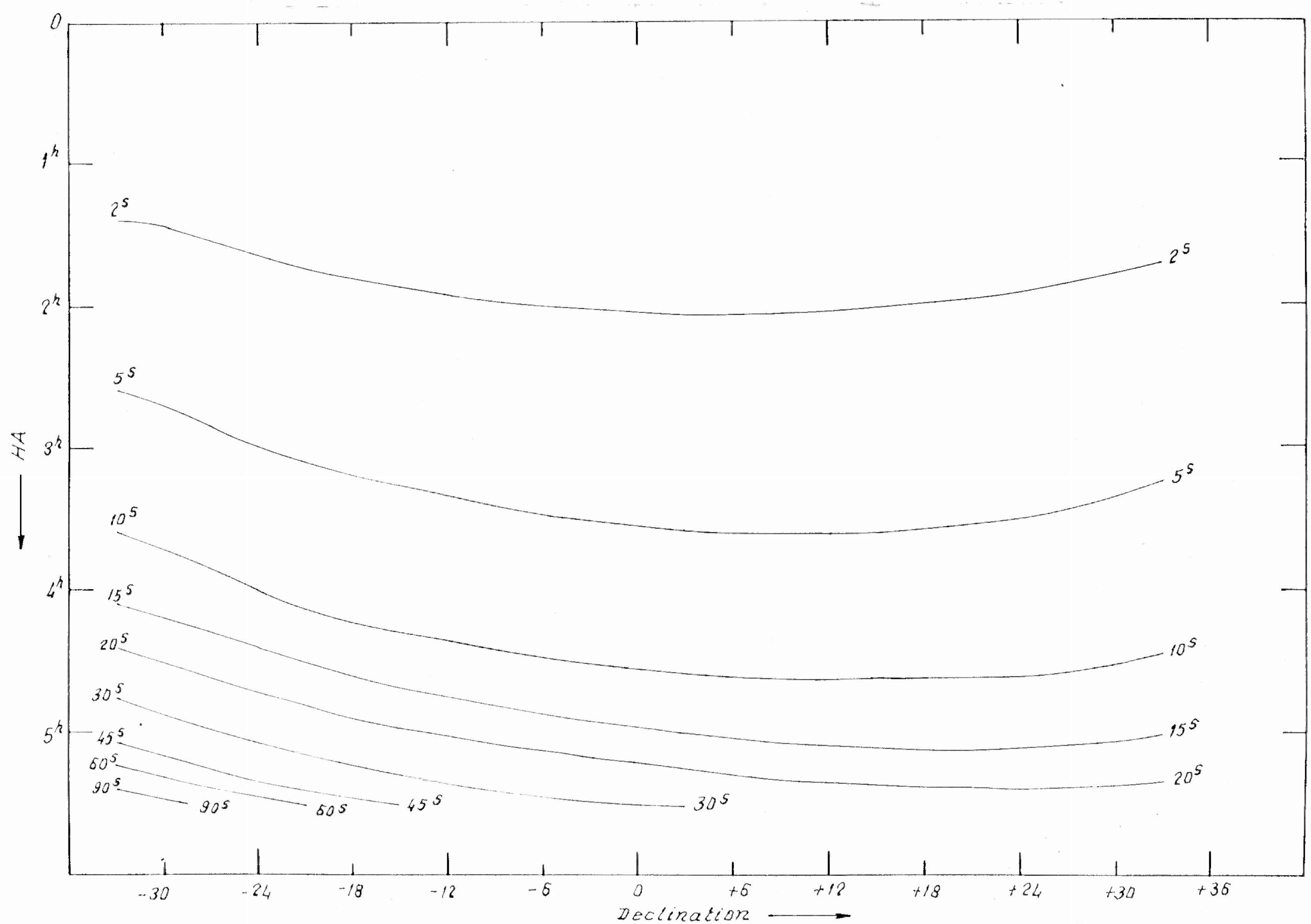

Fig 1.10 Change in ORT hour angle due to refraction at different hour angles and declinations

The extra phase difference between elements A and B due to refraction can be written as

$$\Delta\phi = \frac{2\pi d}{\lambda} (\mu \sin \delta_a - \sin \delta_0)$$

$$= \frac{2\pi d}{\lambda} (\sin \phi\ (\mu \cos Z_a - \cos Z_0) + \cos\phi \cos A_0 (\mu \sin Z_a - \sin Z_0)).$$

The same expression is obtained from the equations in Section 1.3.1 by noting that $A_b=0$ and $z_b=(\pi/2)-\phi$ for ORT, here we take A as the southern element. In the above expression for $\Delta\phi$, contribution of the 2nd term, $d \cos \phi \cos A_0(\mu \sin Z_a - \sin Z_0)$, is very small, in fact it will be zero for a horizontally stratified parallel plane atmosphere, and thus it is finite simply due to the curvature of the atmosphere. While the first term, $d \sin \phi(\mu \cos Z_a - \cos Z_0)$, dominates and is due to the height difference between the north-south elements of ORT. This term is actually the same as derived in Section 1.3.1, but here Z_a also includes the effects due to the curvature of the atmosphere.

This extra phase $\Delta\phi$, if uncorrected for, will result in an apparent southwards shift in the beam-pointing with respect to the source position. Magnitude of this shift can be calculated as

$$\frac{2\pi d \cos \delta}{\lambda} \Delta\delta = \Delta\phi$$

or $$\Delta\delta = \frac{\mu \sin \delta_a - \sin \delta_0}{\cos \delta_0}$$

Thus the source position will appear to shift towards north with respect to the beams; this shift will be larger at large zenith angles and it is also independent of the sign of hour-angle. Fig. 1.11 shows a plot of shift at various hour-angles and declinations. For ORT, the eastern HA

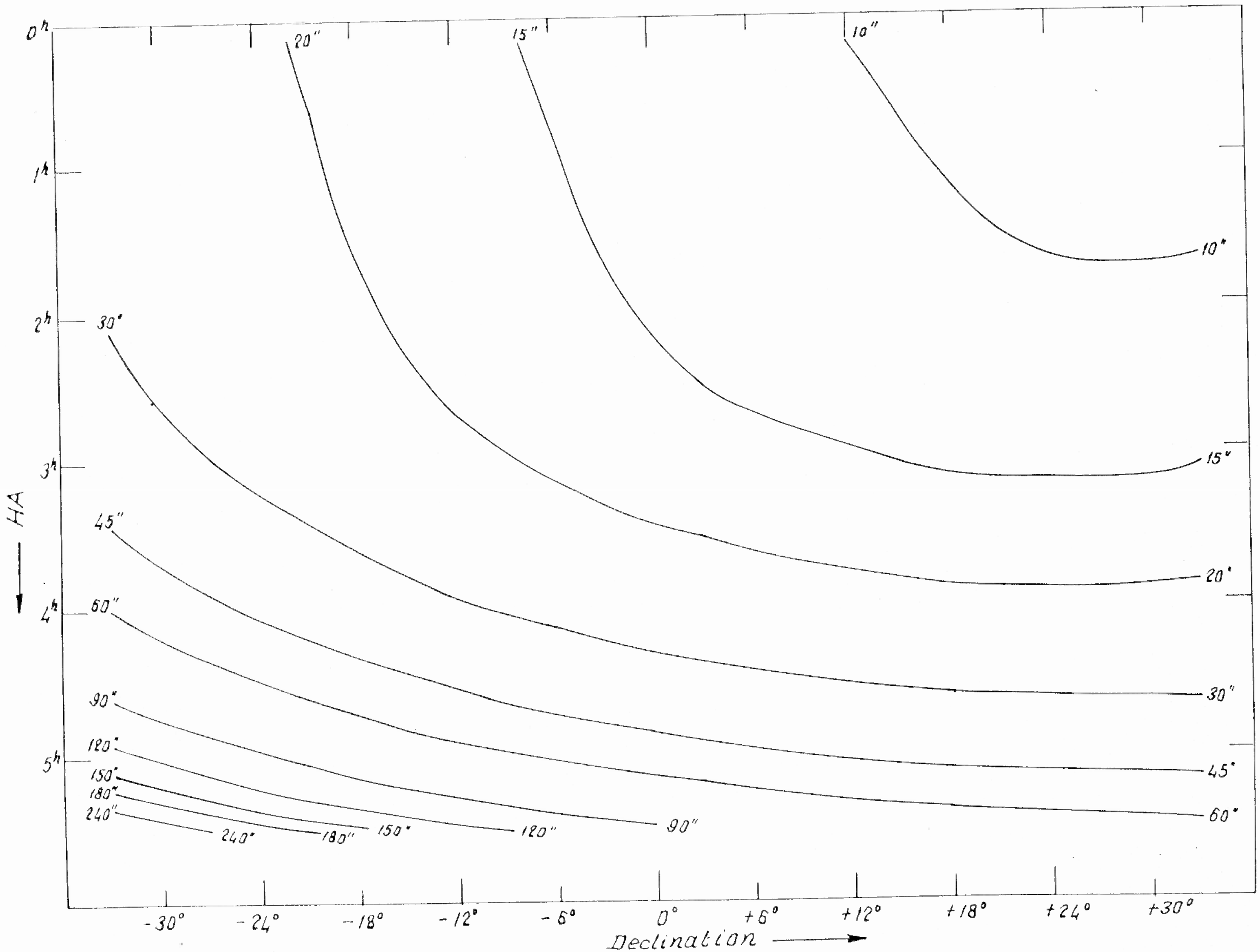

Fig 1.11 Southward shift in ORT beam pointing due to refraction at different hour angles and declinations

limit is at ~ -4^h07^m while the west limit goes up to ~ $+5^h20^m$, so the shift will be more pronounced for a source approaching the west limit. Fig. 1.12 shows some observations and the corresponding predicted shift for the beam position in case of a few sources chosen at different declinations, here a constant shift of 15 arcsec has been subtracted from the predicted value from fig. 1.11. It should be kept in mind that the observations, apart from any other errors, will also be affected by any north-south phasing errors for ORT at the time of observations and the dominant term (due to tropospheric refraction) in predicted values is directly dependent upon any variation in the assumed value of $\mu-1=250X10^{-6}$. Within these uncertainties, the agreement between observations and the predicted values is quite satisfactory. A table of refraction bending for both the ionosphere and the troposphere has been generated and a simple programme has been used above for calculating the errors in declination pointing of ORT.

The formulae of the type given in Section 1.3.1 and 1.3.2 are usuable directly in the pointing routines for the OSRT. Then we would not need to calculate any extra differential phase paths between various antenna elements to account for the refraction effects of average troposphere and ionosphere, these would be automatically taken care of by our procedure. But one needs caution for observations near high zenith angles. The differential bending for a 2°x2° field could be of the order of a few arcmin at high zenith angles, thus causing a considerable distortion in the map in the form of its apparent contraction along the direction towards increasing altitude. This either needs some procedure to compensate for the contraction or it will restrict the hour-angle limit as a function of declination for observations of a source depending upon the width of the field of view and the maximum distortion that can be tolerated in the map.

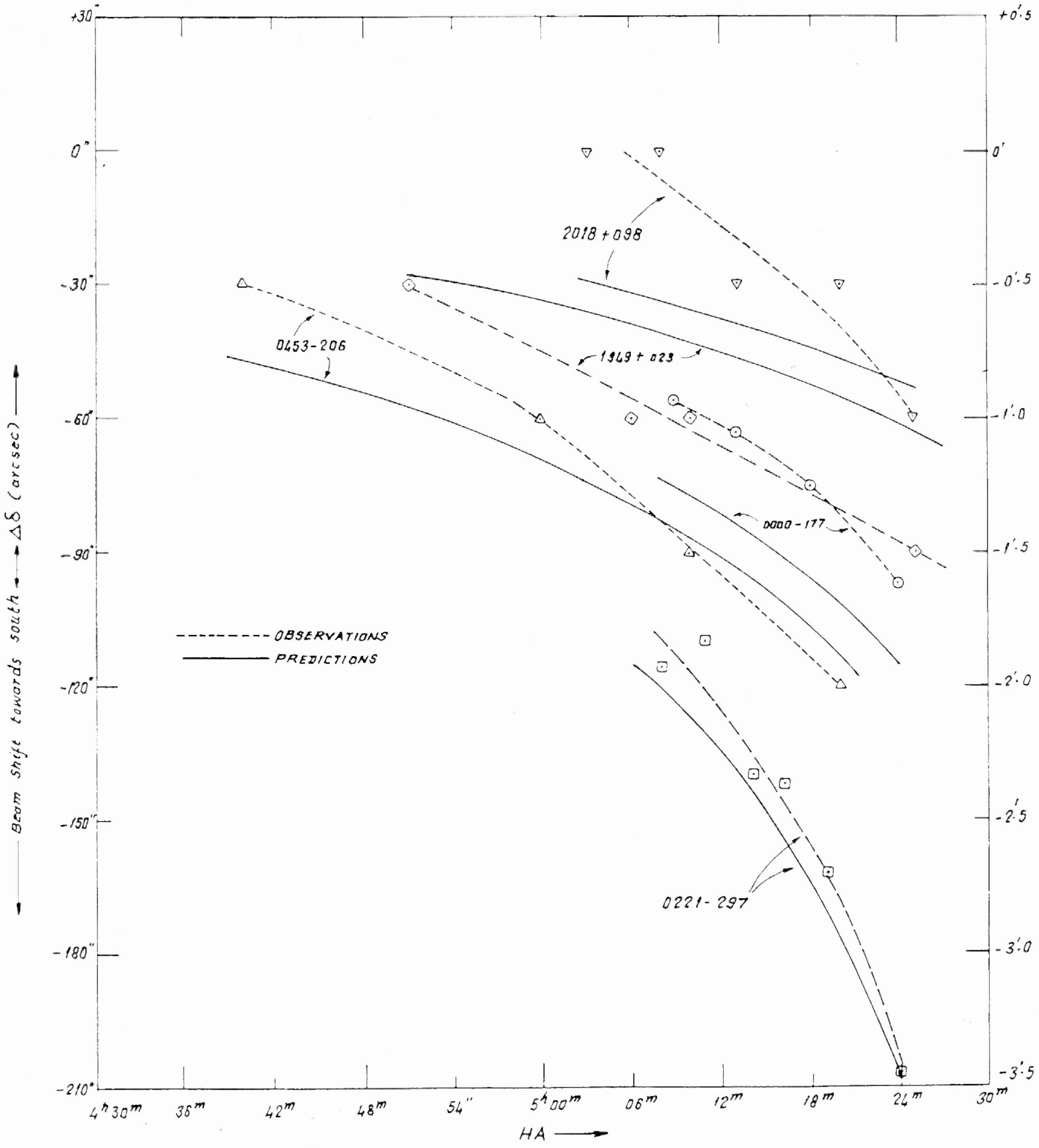

Fig 1.12 Declination pointing error in ORT due to refraction

If the interferometer baseline becomes quite large then the differential bending for the rays reaching two elements may be appreciable. Effectively it implies that the wavefront can no longer be considered planer on the scale of baseline lengths, but it becomes curved due to refraction within the atmosphere. Due to the fact that bending is more at larger zenith angles, the approaching wave front will be always 'concave' as seen by observers on the surface of earth (fig. 1.13). This gives rise to the first order correction to the differential phase path between elements A and B. The differential bending at two elements, with large separation, occurs because the zenith angle of a source is different due to a difference in the longitude and latitude of the two points on the surface of earth, giving rise to a differential refraction. This first order correction gets applied automatically if one uses the midpoint of the baseline as origin for calculating the apparent zenith angle and the azimuth etc. The maximum error, if this effect is uncorrected for, can be estimated in the following way:

The maximum error will occur for the sources which at large zenith angles happen to lie in the vertical plane passing through the baseline. Then the change in differential path $\approx d\sin\theta \cdot \Delta R/2$, where ΔR is the differential bending due to refraction (fig. 1.13). The maximum change in true zenith angle, for a horizontal baseline, from one element to another is d/R_E, where R_E is radius of earth. From figures 1.8 and 1.9, it is estimted that the maximum value of $\Delta R \cdot \sin\theta \lesssim (1/360) d/R_E$ radians. Thus the change in differential path $\lesssim (d^2/2R_E)/360$.

For a 3.5 km baseline this value is $\lesssim$2mm, while for a 9 km baseline it is $\lesssim$2 cm. Thus this change in differential path can be ignored for the OSRT baselines at 326.5 MHz.

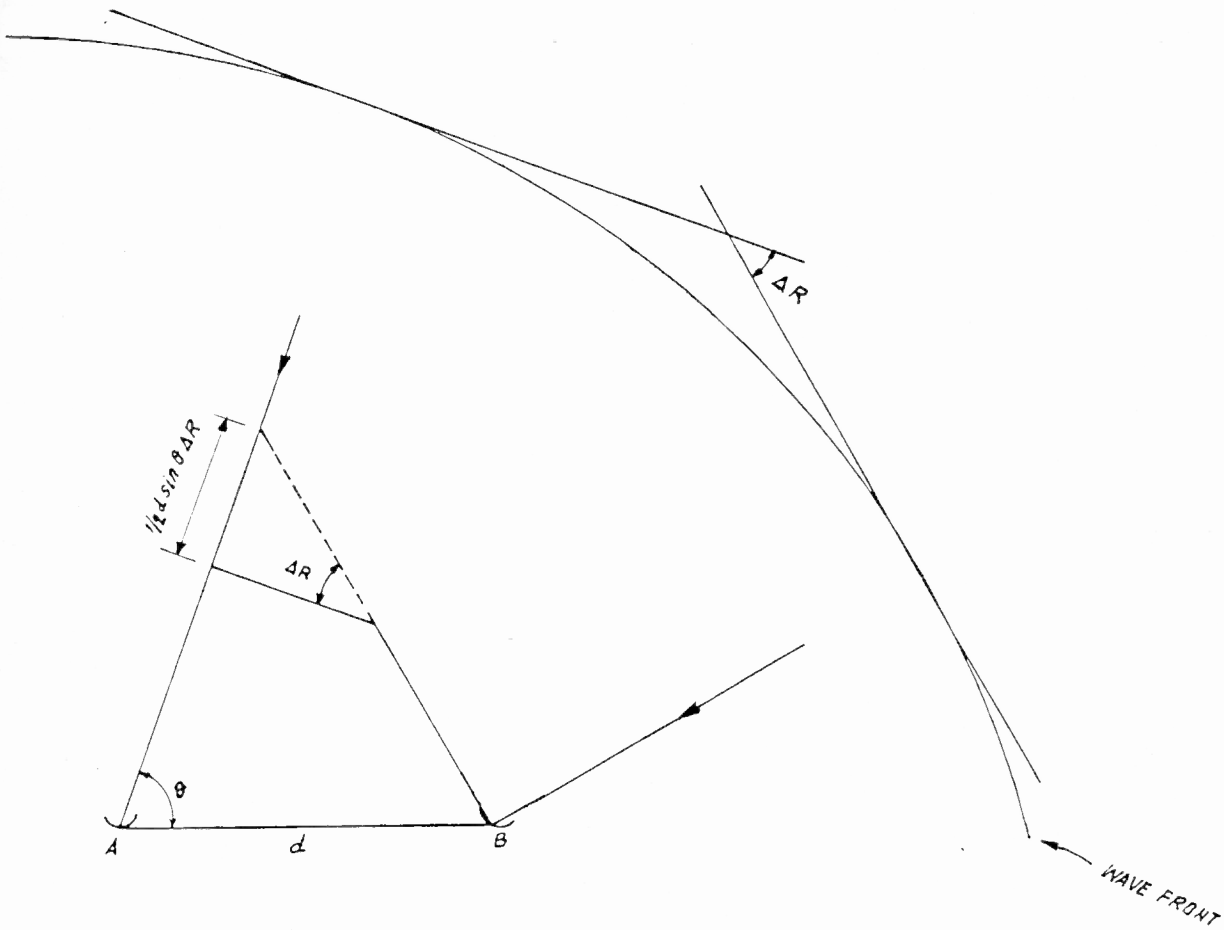

Fig 1.13 Extra phase path between two elements of a long baseline interferometer due to differential bending of wavefront